Arabian Journal of Chemistry (2021) **14**, 103200

King Saud University

Arabian Journal of Chemistry

www.ksu.edu.sa
www.sciencedirect.com

ORIGINAL ARTICLE

Penicillamine functionalized $B_{12}N_{12}$ and $B_{12}CaN_{12}$ nanocages act as potential inhibitors of proinflammatory cytokines: A combined DFT analysis, ADMET and molecular docking study

Yan Cao [a], Afrasyab Khan [b], Hanzaleh Balakheyli [c], Andrew Ng Kay Lup [d], Mohammad Ramezani Taghartapeh [e], Hassan Mirzaei [f], Seyed Reza Khandoozi [g], Alireza Soltani [c], Mehrdad Aghaei [c], Fatemeh Heidari [g], Shaheen M. Sarkar [h], Ahmad B. Albadarin [i,j,*]

[a] *School of Mechatronic Engineering, Xi'an Technological University, Xi'an 710021, China*
[b] *Institute of Engineering and Technology, Department of Hydraulics and Hydraulic and Pneumatic Systems, South Ural State University, Chelyabinsk, Russian Federation*
[c] *Golestan Rheumatology Research Center, Golestan University of Medical Science, Gorgan, Iran*
[d] *School of Energy and Chemical Engineering, Xiamen University Malaysia, Jalan Sunsuria, Bandar Sunsuria, 43900 Sepang, Selangor Darul Ehsan, Malaysia*
[e] *Department of Chemistry and Biotechnology, Swinburne University of Technology, Hawthorn, VIC 3122, Australia*
[f] *Ischemic Disorders Research Center, Golestan University of Medical Sciences, Gorgan, Iran*
[g] *Cancer Research Center, Golestan University of Medical Sciences, Gorgan, Iran*
[h] *Department of Chemical Sciences, Bernal Institute, University of Limerick, Limerick, Ireland*
[i] *Laboratory of Theoretical and Computational Biophysics, Ton Duc Thang University, Ho Chi Minh City, Viet Nam*
[j] *Faculty of Applied Sciences, Ton Duc Thang University, Ho Chi Minh City, Viet Nam*

Received 21 February 2021; accepted 2 May 2021
Available online 18 May 2021

KEYWORDS

Penicillamine;
$B_{12}N_{12}$;
Drug carrier;

Abstract The adsorption of penicillamine (PCA) on pure $B_{12}N_{12}$ and $B_{12}CaN_{12}$ nanocages in aqueous and chloroform solvents has been evaluated using density functional theory (DFT) calculations. The interaction of PCA on $B_{12}N_{12}$ nanocages is chemisorption through its four nucleophilic sites: amine, carbonyl, hydroxyl and thiol. The most stable adsorption configuration was achieved

* Corresponding author at: Ton Duc Thang University, Ho Chi Minh City, Viet Nam (A.B. Albadarin).
E-mail address: ahmad.albadarin@tdtu.edu.vn (A.B. Albadarin).
Peer review under responsibility of King Saud University.

Production and hosting by Elsevier

https://doi.org/10.1016/j.arabjc.2021.103200

Toxicity;
Thermodynamic properties

when zwitterionic PCA adsorbs via its carbonyl group in water with value of −1.723 eV, in contrast, when neutral PCA adsorbs via its amine group in chloroform with value of −1.68 eV. Intercalated calcium ion within $B_{12}N_{12}$ nanocage ($B_{12}CaN_{12}$) was shown to attract PCA onto nanocage surface, resulting in higher solubility and adsorption energy after their complexation in water and chloroform. The adsorption of multiple PCA molecules from their amine and carbonyl groups on pure and $B_{12}CaN_{12}$ nanocages were also evaluated where two and three molecules can be chemisorbed on boron atoms of the nanocage surfaces with the adsorption energy per PCA reduces slightly with the increasing the amount of drugs due to the curvature effects. Molecular docking study indicates that PCA from its NH_2 group on $B_{12}CaN_{12}$ nanocage has the best binding affinity and inhibition potential of tumor necrosis factor-alpha (TNF-α) and Interleukin-1 (IL-1) receptors as compared with the other adsorption systems. Molecular docking and ADMET analysis displayed that the chosen compounds pass Lipinski Rule and have appropriate pharmacokinetic features suitable as models for developing anti-inflammatory agents.

1. Introduction

Penicillamine, *(2S)-2-amino-3-methyl-3-sulfanylbutanoic acid*, is a product from hydrolytic degradation of penicillin. It has four main functional groups: alpha-amine, carbonyl, hydroxyl and thiol which mainly influence its pharmacological effects. Penicillamine has *D*- and *L*-enantiomeric forms in which its *L*-enantiomer is a pyridoxine antagonist has toxic properties, whereas its *D*-enantiomer is an effective oral medication drug for various diseases. It is often used in the treatment of rheumatoid arthritis, Wilson's disease, cystinuria, scleroderma, primary biliary cirrhosis and heavy metal poisoning (Kim and Song, 1997; Joly et al., 1999; Smolarek and Stremmel, 1999). Beside its function as metal chelating agent, PCA also has several important effects such as T-lymphocyte amount reduction, diminishing IL-1, rheumatoid factor reduction, macrophage function inhibition and prevention of collagen cross-linking (Yamanaka et al., 1993; Choy and Panayi, 1999). Nevertheless, PCA can cause a severe allergic reaction in some people and it is associated with adverse effects in 20–40% of patients receiving treatment. Among some of the reported side-effects were myasthenia gravis, thrombocytopenia, dysgeusia rash, pemphigus, hypersensitivity nephritic syndrome. Hence, proper administration of PCA in biological systems is important to ensure maximal drug efficacy and minimal side-effect inducement.

In the recent years, boron nitride (BN) materials as nanoscale drug delivery vehicles have been shown a lot of attention because of good biocompatibility and nontoxicity in biomedical, therapeutic, and diagnostic applications (Ciofani et al., 2010; Ferreira et al., 2013; Ferreira et al., 2011; Horvath et al., 2011). Recently, boron nitride materials are used in the fields of drug delivery, irreversible lethal electroporation cancer treatment, bone tissue engineering and boron neutron capture cancer therapy (Lahiri, 2010; Ciofani et al., 2009; Buzatu et al., 2009). By far, various investigations were done to design rational strategies for the interaction between boron nitride and drug molecules such as 5-fluorouracil (Bezi Javan et al., 2016), 5-aminolevulinic acid (Soltani et al., 2016; Zhu et al., 2020), celecoxib (Abdolahi et al., 2018), 4-aminopyridine (Padash et al., 2018), metformin (Ghasemi et al., 2019) and sulfamide (Padasha et al., 2020). BN materials are relatively more stable in terms of thermal and chemical stability than its carbon nanomaterial counterparts (Abdolhi et al., 2017; Chen et al., 2004; Golberg et al., 2010). Several strategies were proposed on the utilization of BN nanomaterials in various forms such as cluster (Baei et al., 2014; Soltani et al., 2016; Soltani et al., 2018; Abdolahi et al., 2018; Soltani and Baei, 2019; Bezi Javan et al., 2016; Vatanparast and Shariatinia, 2019), nanosheet (Duverger et al., 2019; Carreto Escobar et al., 2019; Chigo Anota et al., 2017; Ebrahimi et al., 2018; Mortazavifar et al., 2019) or nanotubes (Shafiei et al., 2019; Roosta et al., 2016; Soltani et al., 2015; Chigo Anota and Cocoletzi, 2014; Ciofani et al., 2012) as effective drug delivery vehicle.

With the use of BN nanomaterials in biological systems, the study of their interactions with living systems at cellular and sub-cellular levels is important to evaluate their toxicity and their mechanism of action. Ciofani *et al.* evaluated in-vivo toxicological study of boron nitride nanotubes in rabbits to identify acute alteration of hematic parameters. Based on the samples of rabbit blood, their results showed no acute alteration of the assessed parameters after the injection of boron nitride nanotubes (BNNTs) containing solution (1 mg/kg), indicating non-toxicity of BNNT solution at the correct administered dosage (Emanet et al., 2015). Likewise, Emanet *et al.* investigated on the cytotoxicity and genotoxicity of carbohydrate modified BNNTs on human dermal fibroblasts (HDFs) and adenocarcinoma human alveolar basal epithelial cells (A549) where no significant viability change and DNA damage of HDFs and A549 cells were reported. (Mirmotahari et al., 2019). In particular, Mirmotahari *et al.* have theoretically demonstrated that the Calcium-doped single-wall nanotubes (Ca/SWCNTs) as a superior carrier for the improvement of the solubility and stability of atropine drug in the water solvent (Sui et al., 2018). They found that the strong adsorption of *D*- and *L*-atropine molecules with the surface of Ca/SWCNT through O–Ca bond could improve the solubility and stability of drugs along with Ca/SWCNT in the water after their complexation. Sui *et al.* reported Ca^{2+} in MBG nanospheres activates transient receptor potential (TRP) channels and calcium-sensing receptor (CaSR) on tumor cells, mediates calcium influx, and directly regulates the Calpain-1-Bcl-2-Caspase-3 signaling pathway to specifically suppress tumor growth without affecting normal cells (Zhao et al., 2006). In the light of these findings, we propose in this study

the use of calcium functionalized $B_{12}N_{12}$ nanocage as a potential drug delivery vehicle for penicillamine. The intercalation of calcium in $B_{12}N_{12}$ nanocage was postulated to improve the stability and the solubility of PCA/ $B_{12}CaN_{12}$ complex. This intercalation was also further motivated on *a priori* basis that calcium ions are commonly found in living organisms thus endorsing a certain extent of its biocompatibility. The interactions of penicillamine with $B_{12}N_{12}$ and $B_{12}CaN_{12}$ nanocages were examined using computational methods based on several perspectives. In Section 3.1, equilibrium geometries, energetics of the neutral and the zwitterionic PCA molecules interacting with the surface of bare $B_{12}N_{12}$ and $B_{12}CaN_{12}$ cages were discussed in both vacuum and aqueous environments. In Sections 3.2 and 3.3, discussions on thermodynamic parameters, vibrational assignments, quantum molecular descriptors and electronic features of the adsorption complexes were presented. In Section 3.4, interaction of PCA/$B_{12}N_{12}$ complexes with protein tumor necrosis (TNF-α) and interleukin-1 (IL-1) were discussed so as to investigate their role in reducing the levels of proinflammatory cytokines TNF-α and IL-1.

2. Computational methods

The geometries of the pure and calcium functionalized $B_{12}N_{12}$ fullerene-like cages, PCA molecule and their interaction configurations with different orientations have been fully relaxed by using Minnesota 2006 with double-Hartree-Fock-exchange functional (M06-2X) in conjunction with 6-311G** basis set for both chloroform and water solvent system (Xu et al., 2014; Schmidt et al., 1993). The polarizable continuum model (PCM) was selected to evaluate the impact of the solvent on the adsorption behavior of the PCA drug in water and chloroform. Moreover, total density of states (TDOS), frontier molecular orbital (FMO), molecular electrostatic potential (MEP), and natural bond orbital (NBO) analysis were performed using GAMMAS structural package (Blaudeau et al., 1997). Here, the basis set superposition errors (BSSE) were resolved by calculating the BSSE energy (E_{BSSE}) for all adsorption configurations. The accuracy of computations was further verified by performing the optimizations with dispersion-corrected *meta*-GGA hybrid i.e., M06-2X-D technique that yielded the differences in the qualitative results (Rassolov et al., 1998; Jamroz, 2004–2010.). The adsorption energies (E_{ads}) were calculated using the following equation:

$$E_{ads} = E_{PCA/Cage} - \left(E_{cage} + E_{PCA}\right) + E_{BSSE} \tag{1}$$

where E_{cage} is the total energy of pure or calcium functionalized $B_{12}N_{12}$ fullerene-like cage, E_{PCA} is the total energy of isolated PCA molecule and $E_{PCA/Cage}$ is the total energy of the adsorption complex.

Vibrational frequencies were also evaluated at M06-2X functional with 6-311G** basis set to check the reliability of the relaxed structure, as well as to help assign experimental IR transitions with further studies of all possible vibrational assignments using VEDA software (Parr et al., 1978). The thermodynamics of PCA adsorption on $B_{12}N_{12}$ and $B_{12}CaN_{12}$ nanocage was also examined based on the Gibbs free energy change ($\Delta_{ads}G$), enthalpy change ($\Delta_{ads}H$) and entropy change ($\Delta_{ads}S$) per molecule during adsorption. These thermodynamic parameters were determined at 298 K and 1 atm using B3LYP functional with 6–31 + + G** basis set. Gibbs-Helmholtz relation was used to relate $\Delta_{ads}G$ with adsorption equilibrium constant, K_{ads}. The analysis of the temperature dependence of K_{ads} was examined using van 't Hoff equation (Eq. (2)) and van't Hoff plot.

$$lnK_{ads} = -\frac{\Delta_{ads}H}{R}\left(\frac{1}{T}\right) + \frac{\Delta_{ads}S}{R} \tag{2}$$

Physicochemical properties of the adsorption complexes were also predicted based on the determination of quantum molecular descriptors:

$$\mu = -\frac{1}{2}(I + A) \tag{3}$$

$$\chi = -\mu \tag{4}$$

$$\eta = \frac{1}{2}(I - A) \tag{5}$$

$$S = \frac{1}{2\eta} \tag{6}$$

$$\omega = \frac{\mu^2}{2\eta} \tag{7}$$

where I is ionization potential, A is electron affinity, μ is chemical potential, χ is electronegativity, η is global hardness, S is global softness and ω is electrophilicity index (Parr et al., 1999; Koopmans, 1933). Based on Koopmans' theorem, I and A can be respectively approximated as the negative orbital energies of the highest occupied molecular orbital (HOMO), $-E_{HOMO}$ and the lowest unoccupied molecular orbital (LUMO),$-E_{LUMO}$ (Morris et al., 2009).

Molecular docking analysis was conducted via Auto Dock package (4.2) (Mirzaei et al., 2017). The crystal structures of TNF-alpha (PDB ID: 2AZ5) and IL1A-S100A13 (PDB ID: 2L5X) were obtained from Protein Data Bank. Lamarckian genetic algorithm was employed for local search method. Grid map of 60 × 60 × 60 with 0.375 Å grid spacing were designated for preparation of autogrid (Mirzaei et al., 2017; He et al., 2005). 100 GA runs was used for docking. Maestro 11.0 Schrodinger program was applied for creation of 2D and 3D presentations. Hence for validation of the docking protocol, the co-crystallized ligand was also re-docked. The root mean square deviation (RMSD) of the cognate ligand atoms in the re-docked and crystallographic conformations was 0.994 Å. The best docking solutions were chosen for further studies in this work (Mohan and Yu, 2011; Shaki et al., 2020).

3. Result and discussion

3.1. Interaction of PCA molecule on the surfaces of $B_{12}N_{12}$ and $B_{12}CaN_{12}$ cages

The geometry optimization of PCA/$B_{12}N_{12}$ adsorption system shows six stable adsorption complexes (Fig. 3). Four of these complexes were formed by neutral PCA molecule via its four nucleophilic sites (Fig. 1): amine (Complex A), carbonyl (Complex B), hydroxyl (Complex C) and thiol (Complex D). The other two complexes were formed by zwitterionic PCA via its carbonyl (Complex E) and hydroxyl (Complex F) groups. All adsorption configurations were of chemisorption nature

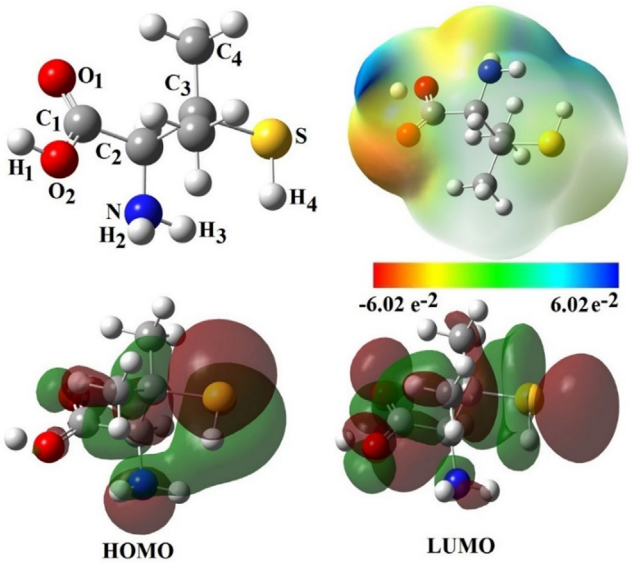

Fig. 1 Optimized structure, MEP and FMO plots of penicillamine.

as the interactions showed a strong overlapping of electrons between the cages and drug molecule as shown by the NBO analysis. The electrons overlapping was formed through the lone pair electrons of the PCA nucleophilic sites with the empty valence *p* orbital of boron in $B_{12}N_{12}$ cage as the Lewis acid site. MEP map is a significant tool to find the active sites for electrophilic and nucleophilic attacks in the biological recognition process and hydrogen bonding interactions. The boron atom of $B_{12}N_{12}$ is blue color (positive electrostatic potential region) functions as the active site to adsorb PCA through the NH_2 and C = O groups with red color (negative electrostatic potential region).

Based on Tables 1 and 2, Complex A and E are the most stable adsorption configuration for PCA in the respective neutral and zwitterionic forms with the respective adsorption energies of −1.715 eV and −1.724 eV in aqueous environment or −1.68 eV and −1.41 eV in chloroform environment which are in corroboration with previous literature reports (Ghasemi et al., 2018; Kokalj et al., 2020). Complex E ($E_{ads} = -1.724eV, -1.41eV$) and F ($E_{ads} = -1.482eV, -1.48eV$) were noted to have higher adsorption energy and stability than their counterparts: Complex B ($E_{ads} = -1.213eV, -1.23eV$) and C ($E_{ads} = -0.304eV, -0.32eV$) in both solvent environments. This is because the charges in NH_3^+ and COO^- groups of zwitterionic PCA can be further stabilized by the hydrogen bonding provided by the solvents. By the same token, one would also expect the adsorption configuration via amine and carbonyl groups to be more stable as compared with hydroxyl and thiol groups (Bieri and Thomas Bürgi, 2006) as shown in Tables 1 and 2. S-zwitterionic PCA which involves the formation of NH_3^+ and S^- groups was not one of the stable adsorption configurations albeit it was reported to be possibly formed on other adsorbents (Ammar et al., 2019).

In neutral form, Complex C and D were noted to be significantly weaker than Complex A and B. In Complex C, the hydrogen in neutral hydroxyl group restricts the availability of lone pair electron in oxygen atom for chemisorption as compared with its deprotonated form. Thus, one would expect a significant increase in adsorption energy from −0.304 eV to −1.482 eV in water and −0.32 eV to −1.48 eV in chloroform during the deprotonation of OH group (Complex C) into O^- group (Complex F). As for Complex D, the larger sulfur atomic size will increase the chemisorbed bond length thereby effectively weakens the bond despite having the highest charge transfer (0.457 |e|) among the other adsorption heads. By switching from water to chloroform solvent, miniscule reduction in the adsorption energies and the bond lengths was observed which could be attributed to both solvents with hydrogen bonding capacity. In regard to the solvent polarity, chloroform has lower polarity than water which exhibits lesser polarization and hence lower dipole moment of the adsorption system as compared with aqueous environment (Nagarajan and Chandiramouli, 2019).

For a better simulation of the real adsorption environment within the experimental preparation of the adsorption system

Table 1 Calculated adsorption energy (E_{ads}), chemisorption bond distance (D), dipole moment (μ_D), HOMO energy (E_{HOMO}), LUMO energy (E_{LUMO}), energy gap (E_g), Fermi level energy (E_F) and quantum molecular descriptors for PCA, $B_{12}N_{12}$, $B_{12}CaN_{12}$, PCA/$B_{12}N_{12}$ and PCA/ $B_{12}CaN_{12}$ in aqueous environment.

Property	$E_{ads}(eV)$	D()	$\mu_D(Debye)$	$E_{HOMO}(eV)$	$E_{LUMO}(eV)$	$E_g(eV)$	$\Delta E_g(\%)$	$E_F(eV)$	$I(eV)$	$A(eV)$	$\chi(eV)$	$\mu(eV)$	$\eta(eV)$	$S(eV^{-1})$	$\omega(eV)$
PCA	–	–	3.54	−8.31	0.76	9.07	–	−3.78	8.31	−0.76	3.78	−3.78	4.54	0.110	1.57
$B_{12}N_{12}$	–	–	0.0	−9.44	0.07	9.51	–	−4.69	9.44	−0.07	4.69	−4.69	4.76	0.105	2.31
A	−1.715	1.62	10.20	−8.69	0.28	8.97	5.68	−4.21	8.69	−0.28	4.21	−4.21	4.49	0.111	1.97
B	−1.213	1.53	7.13	−8.47	−0.41	8.06	15.25	−4.44	8.47	0.41	4.44	−4.44	4.03	0.124	2.45
C	−0.304	1.68	3.78	−8.44	−0.37	8.07	15.14	−4.41	8.44	0.37	4.41	−4.41	4.04	0.124	2.40
D	−0.642	2.07	9.81	−8.68	0.30	8.98	5.57	−4.19	8.68	−0.30	4.19	−4.19	4.49	0.111	1.96
E	−1.724	1.49	22.56	−8.51	0.29	8.80	7.46	−4.11	8.51	−0.29	4.11	−4.11	4.40	0.114	1.92
F	−1.482	1.48	13.82	−8.66	0.27	8.93	6.10	−4.20	8.66	−0.27	4.20	−4.20	4.47	0.112	1.97
G	−1.209	1.60	12.71	−8.34	−0.42	7.92	16.72	−4.38	8.34	0.42	4.38	−4.38	3.96	0.126	2.42
H	−1.533	1.64	15.55	−8.29	0.34	8.63	9.25	−3.98	8.29	−0.34	3.98	−3.98	4.32	0.116	1.83
I	−1.499	1.63	8.44	−7.83	0.39	8.22	13.56	−3.72	7.83	−0.39	3.72	−3.72	4.11	0.122	1.68
Ca-$B_{12}N_{12}$	+5.35	2.69	14.75	−4.47	−1.31	3.46	63.62	−3.04	4.47	1.31	2.89	−2.89	1.58	0.316	2.64
J	−2.162	1.59	21.39	−4.48	−0.9	3.58	3.47	−2.69	4.48	0.90	2.69	−2.69	1.79	0.279	2.02
K	−2.049	1.61	24.69	−4.18	−0.39	3.79	9.54	−2.29	4.18	0.39	2.29	−2.29	1.90	0.264	1.38
L	−2.018	1.60	26.66	−3.91	0.0	3.91	13.0	−1.96	3.91	0	1.96	−1.96	1.96	0.256	0.98

Table 2 Calculated adsorption energy (E_{ads}), chemisorption bond distance (D), dipole moment (μ_D), HOMO energy (E_{HOMO}), LUMO energy (E_{LUMO}), energy gap (E_g), Fermi level energy (E_F) and quantum molecular descriptors for PCA, $B_{12}N_{12}$, $B_{12}CaN_{12}$, PCA/$B_{12}N_{12}$ and PCA/ $B_{12}CaN_{12}$ in chloroform environment.

	$E_{ads}(eV)$	$D()$	$\mu_D(Debye)$	$E_{HOMO}(eV)$	$E_{LUMO}(eV)$	$E_g(eV)$	$\Delta E_g(\%)$	$E_F(eV)$	$I(eV)$	$A(eV)$	$\chi(eV)$	$\mu(eV)$	$\eta(eV)$	$S(eV^{-1})$	$\omega(eV)$
PCA	–	–	3.23	−8.29	0.78	9.07	–	−3.76	8.29	−0.78	3.76	−3.76	4.54	0.110	1.55
$B_{12}N_{12}$	–	–	0.0	−9.44	0.04	9.48	–	−4.70	9.44	−0.04	4.70	−4.70	4.74	0.105	2.33
A	−1.68	1.63	9.93	−8.71	0.22	8.93	5.80	−4.25	8.71	−0.22	4.25	−4.25	4.47	0.112	2.01
B	−1.23	1.53	6.67	−8.53	−0.41	8.12	14.35	−4.47	8.53	0.41	4.47	−4.47	4.06	0.123	2.46
C	−0.32	1.72	3.30	−8.48	−0.35	8.13	14.24	−4.42	8.48	0.35	4.42	−4.42	4.07	0.123	2.40
D	−0.661	2.06	9.20	−8.63	0.33	8.98	5.48	−4.15	8.63	−0.33	4.15	−4.15	4.48	0.112	1.92
E	−1.41	1.49	12.79	−8.50	0.17	8.67	8.54	−4.17	8.50	−0.17	4.17	−4.17	4.34	0.115	2.00
F	−1.48	1.51	11.55	−8.26	0.22	8.48	10.55	−4.02	8.26	−0.22	4.02	−4.02	4.24	0.118	1.91
G	−1.17	1.61	11.32	−8.21	−0.42	7.79	17.83	−4.32	8.21	0.42	4.32	−4.32	3.90	0.128	2.39
H	−1.50	1.64	13.66	−8.18	0.30	8.48	10.55	−3.94	8.18	−0.30	3.94	−3.94	4.24	0.118	1.83
I	−1.46	1.65	7.04	−7.63	0.41	8.04	15.19	−3.61	7.63	−0.41	3.61	−3.61	4.02	0.124	1.62
Ca-$B_{12}N_{12}$	+5.75	2.72	12.17	−4.55	−1.33	3.22	66.03	−2.94	4.55	1.33	2.94	−2.94	1.61	0.311	2.68
J	−2.23	1.61	18.70	−4.11	−0.85	3.26	1.24	−2.48	4.11	0.85	2.48	−2.48	1.63	0.307	1.89
K	−1.97	1.61	11.33	−3.76	−0.26	3.50	8.70	−2.01	3.76	0.26	2.01	−2.01	1.75	0.286	1.15
L	−1.92	1.62	21.09	−3.30	0.11	3.41	5.90	−1.60	3.30	−0.11	1.60	−1.60	1.71	0.293	0.75

as well as the body for real clinical testing, the adsorption of multiple PCA molecules on the outer surface of $B_{12}N_{12}$ nanocage was performed in both water and chloroform environments (Srimathi et al., 2018; Raggi et al., 2014). Based on the most stable adsorption configuration of neutral PCA (Complex A), two types of adsorption configuration were considered for the second PCA molecule: carbonyl (Complex G) and amine (Complex H) as shown in Fig. 3. It is confirmed that the most important adsorption configuration corresponds to the two PCA molecules interacting from their amine groups onto the boron site of $B_{12}N_{12}$ nanocage with adsorption energy per PCA molecule and NBO charge of −1.533 eV and 0.18 |e|

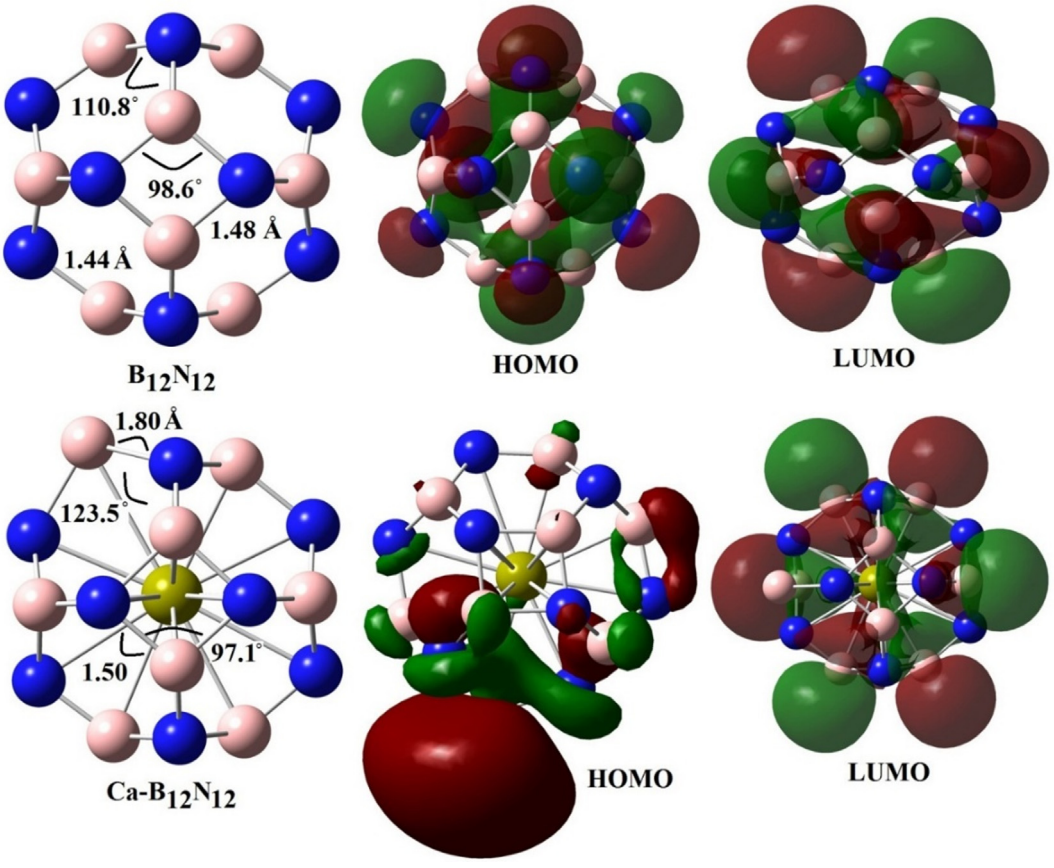

Fig. 2 Optimized structures and FMO plots of $B_{12}N_{12}$ and $B_{12}CaN_{12}$ nanocages.

or −1.50 eV and 0.16 |e| in water or chloroform environment. For three PCA molecules system, the most stable complex is formed with adsorption configuration involving three consecutive amine groups from three PCA molecule with the adsorption energy per PCA molecule and NBO charge of −1.499 eV and 0.17 |e| or −1.460 eV and 0.17 |e| in water or chloroform environments. As the number of PCA molecule adsorbed on nanocage increases, steric effect becomes more prominent, causing the stability of adsorption complex to decrease. Such effect could be seen through the gradual decrease in adsorption energy per PCA molecule for Complex A (−1.715 eV, −1.68 eV), H (−1.533 eV, −1.50 eV) and I (−1.499 eV, −1.46 eV) in both environments.

The geometry optimizations of the $B_{12}CaN_{12}$ nanocage adsorbent were also carried out in both water and chloroform environments. Three stable PCA/$B_{12}CaN_{12}$ complexes were formed with successive adsorption of PCA molecules via amine group: single (Complex J), double (Complex K) and triple (Complex L). It was found that the positively charged encapsulated calcium (Ca) ion with a point charge of + 0.97 |e| is located at a radial distance of 2.29 Å away from the center of $B_{12}N_{12}$ nanocage and facing the midpoint of an edge between the two adjacent hexagon and square sites of the nanocage. The exohedral intercalation of Ca ion has caused the bond length of the 4-member ring of BN nanocage to increase from 1.48 Å to 1.50 Å while its bond angle to decrease from 98.6° to 97.1°. Plane distortion was also noted via the displace of a boron atom from the 5-member ring causing the bond length and the bond angle to increase from 1.44 Å to 1.80 Å and 110.8° to 123.5° respectively (Fig. 2). The position of Ca ion inside the $B_{12}N_{12}$ has a critical influence on the polarization and symmetry of the nanocage, which is similar with the obtained results by Raggi *et al* (Cazorla et al., 2012). It was found that the encapsulated Ca ion inside the $B_{12}N_{12}$ nanocage can outstandingly shift the value of the dipole moment from zero to 14.75 (water) or 12.17 (chloroform). This effect can be attributed to the positive charge of calcium ion and the displacement of boron atom from $B_{12}N_{12}$ which breaks the centrosymmetry of pristine $B_{12}N_{12}$: an essential property for its equal charge distribution.

Based on Tables 1 and 2, calcium functionalization has also resulted in the reduction of HOMO-LUMO energy gap and the global hardness of nanocage, thus enabling a more facile interaction with PCA molecule. The complexation of PCA/$B_{12}CaN_{12}$ was carried out and it was found that the stable adsorption configurations were also similarly achieved via amine group. The intercalation of Ca ion in fullerene effectively attracts the PCA molecule toward the surface, thus further stabilizing the adsorption complex (Nejati et al., 2017). The obtained adsorption energies of the multiple PCA drugs via its amine groups is much stronger than that from the combined amine and carbonyl groups (Li et al., 2019; Yongnian et al., 1998). Similar steric effect in PCA/$B_{12}CaN_{12}$ system was also observed in both environments where the stability of adsorption complex decreases as the number of adsorbing PCA molecule increases: Complex J (Single PCA) with $E_{ads} = -2.162eV, -2.23eV >$ Complex K (Double PCA) with $E_{ads} = -2.049eV, -1.97eV >$ Complex L (Triple PCA) with $E_{ads} = -2.018eV, -1.92eV$. However, if one was to compare with PCA/$B_{12}N_{12}$ system, $B_{12}CaN_{12}$ provides greater adsorption capacity at a relatively higher stability.

Table 3 Calculated stretching vibration wavenumber (ν), enthalpy change ($\Delta_{ads}H$), Gibbs free energy change ($\Delta_{ads}G$), entropy change ($\Delta_{ads}S$) and thermodynamic equilibrium constant (K_{ads}) of adsorption at 298 K and 1 atm.

	$\Delta_{ads}H(eV)$	$\Delta_{ads}G(eV)$	$\Delta_{ads}S(eV/K)$	K_{ads}	$\nu_{min}(cm^{-1})$	$\nu_{max}(cm^{-1})$	$\nu_{B-N}(cm^{-1})$	$\nu_{C=O}(cm^{-1})$	$\nu_{N-H}(cm^{-1})$	$\nu_{S-H}(cm^{-1})$	$\nu_{NH_2}(cm^{-1})$	$\nu_{O-H}(cm^{-1})$
PCA	–	–	–	–	45	3814	–	1872	3542	2760	1643	3814
$B_{12}N_{12}$	–	–	–	–	326	1466	1441	–	–	–	–	–
A	−1.50	−0.90	−0.0020	1.67×10^{15}	27	3805	1446	1894	3513	2758	1632	3705
B	−1.24	−0.64	−0.0020	6.70×10^{10}	27	3628	1436	1695	3539	2774	1653	3628
C	−0.31	+0.25	−0.0019	5.90×10^{-5}	22	3729	1438	1940	3519	2770	1661	3632
D	−0.53	+0.04	−0.0019	2.11×10^{-1}	31	3797	1442	1866	3545	–	1632	3645
E	−1.03	−0.43	−0.0020	1.88×10^{7}	30	3495	1446	1810	3389	2743	1660	–
F	−0.77	−0.14	−0.0021	2.33×10^{2}	21	3519	1449	1879	3413	2764	1644	–
Ca-$B_{12}N_{12}$	–	–	–	–	196	1362	1329	–	–	–	–	–
J	−1.89	−1.30	−0.0020	9.77×10^{21}	26	3795	1351	1893	3487	2758	1635	3769

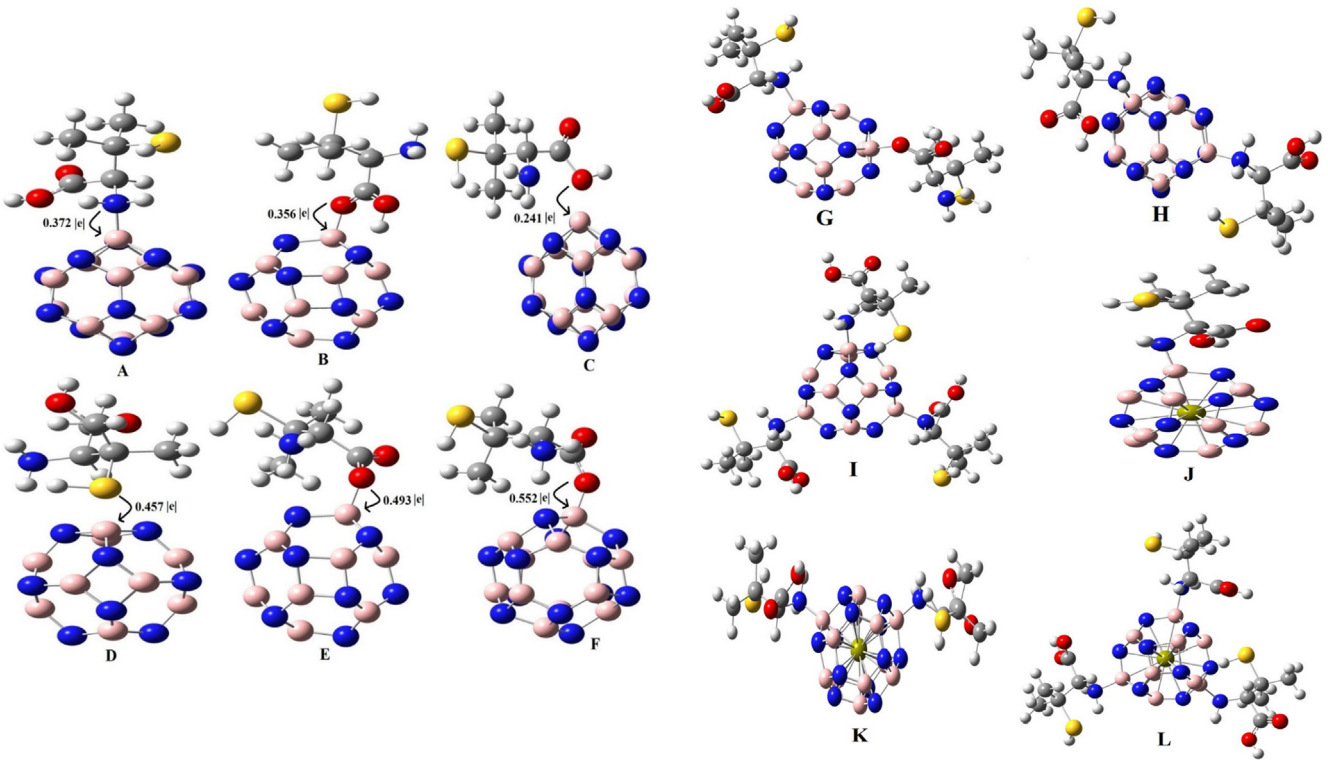

Fig. 3 Adsorption of neutral PCA on $B_{12}N_{12}$ via amine (A), carbonyl (B), hydroxyl (C), thiol (D) groups; zwitterionic PCA on $B_{12}N_{12}$ via carbonyl (E), hydroxyl (F) groups and multiple neutral PCAs on $B_{12}CaN_{12}$ (G – L).

3.2. Vibrational assignments and thermodynamic parameters

Infrared and thermodynamic analyses were computationally calculated for all relaxed structures of PCA/$B_{12}N_{12}$ and PCA/ $B_{12}CaN_{12}$ systems (Table 3). The C = O, N-H, S-H, NH_2 bending vibration and O-H bonds of PCA molecule were reported to have stretching vibration wavenumbers of 1872 cm^{-1}, 3542 cm^{-1}, 2760 cm^{-1}, 1643 cm^{-1} and 3814 cm^{-1} respectively, which are agree with the experimental results reported by Li *et al* (Seifert et al., 1997). Upon adsorption, the stretching vibration modes of PCA molecule were slightly decreased by 6 to 200 cm^{-1}. Such decrease would indicate the weakening of the covalent character of existing bonds in PCA during chemisorption. This effect was noted to affect the energy mode of the entire PCA molecule as the non-chemisorbed bonds of PCA also experience a slight reduction in vibration energies to different extents. On the flip side, the B-N bond wavenumber of $B_{12}N_{12}$ molecule remained within the range of 1436 cm^{-1} to 1449 cm^{-1} during the interaction which is quite close to its initial wavenumber of 1441 cm^{-1}. The experimental FT-IR spectrum shows the two characteristic absorption bands at 1380 cm^{-1} (in plane B-N stretching) and 780 cm^{-1} (out-of-plane B-N-B bending) of h-BN crystal structure (Shokuhi Rad and Aghaei, 2018). This very much indicates of the independency of the interacting BN bond from the rest of BN bonds within the nanocage. Another possible explanation would be that the vibrational shift of the interacting BN bond was averaged out by the unchanged vibrational mode of the non-interacting BN bonds of nanocage. With the intercalation of calcium ion, vibrational wavenumber of BN bonds were reduced from 1441 cm^{-1} to 1329 cm^{-1} which indicates the existing BN bonds were weakened as they form partial bonds with the calcium ions.

For all complexes, the $\Delta_{ads}H$ values were noted to be significant with the range of −0.31 to −1.89 eV per molecule. This corroborates with the large adsorption energy trend in indicating the chemisorption of PCA on $B_{12}N_{12}$ and $B_{12}CaN_{12}$ nanocages and the formation of stable adsorption complexes. All adsorption configurations also experienced similar range of entropy reduction (-0.0019 to −0.0021 eV/K) which is attributed to the reduced vibrational energies during adsorption (Vessally et al., 2017). This effect is evident particularly in the bonds of the four functional groups of PCA molecule. The lesser values of $\Delta_{ads}G$ than $\Delta_{ads}H$ were due to the entropic reduction effect. Based on the $\Delta_{ads}G$ and K_{ads} values at 298 K, PCA adsorption is exergonic and thermodynamically favored for Complex A, B, E, F and J ($\Delta_{ads}G < 0$ and $K_{ads} > 1$) whereas PCA adsorption is endergonic and not thermodynamically favored for Complex C and D ($\Delta_{ads}G > 0$ and $K_{ads} < 1$). Thermodynamic analysis shows that the adsorption of PCA on $B_{12}N_{12}$ via its amine group has the largest values of $\Delta_{ads}H$ (−1.50 eV) and $\Delta_{ads}G$ (−0.90 eV) as compared with other adsorption configurations. This corroborates with the preceding discussion on its largest adsorption energy is indicating it as the most stable adsorption configuration of PCA/$B_{12}N_{12}$ system.

Fig. 4 demonstrates the van 't Hoff plots for PCA/$B_{12}N_{12}$ and PCA/ $B_{12}CaN_{12}$ systems with T_i^+ as the respective temperature which gives no change in Gibbs free energy during the i^{th} adsorption. At 298 K, all adsorption complexes are enthalpi-

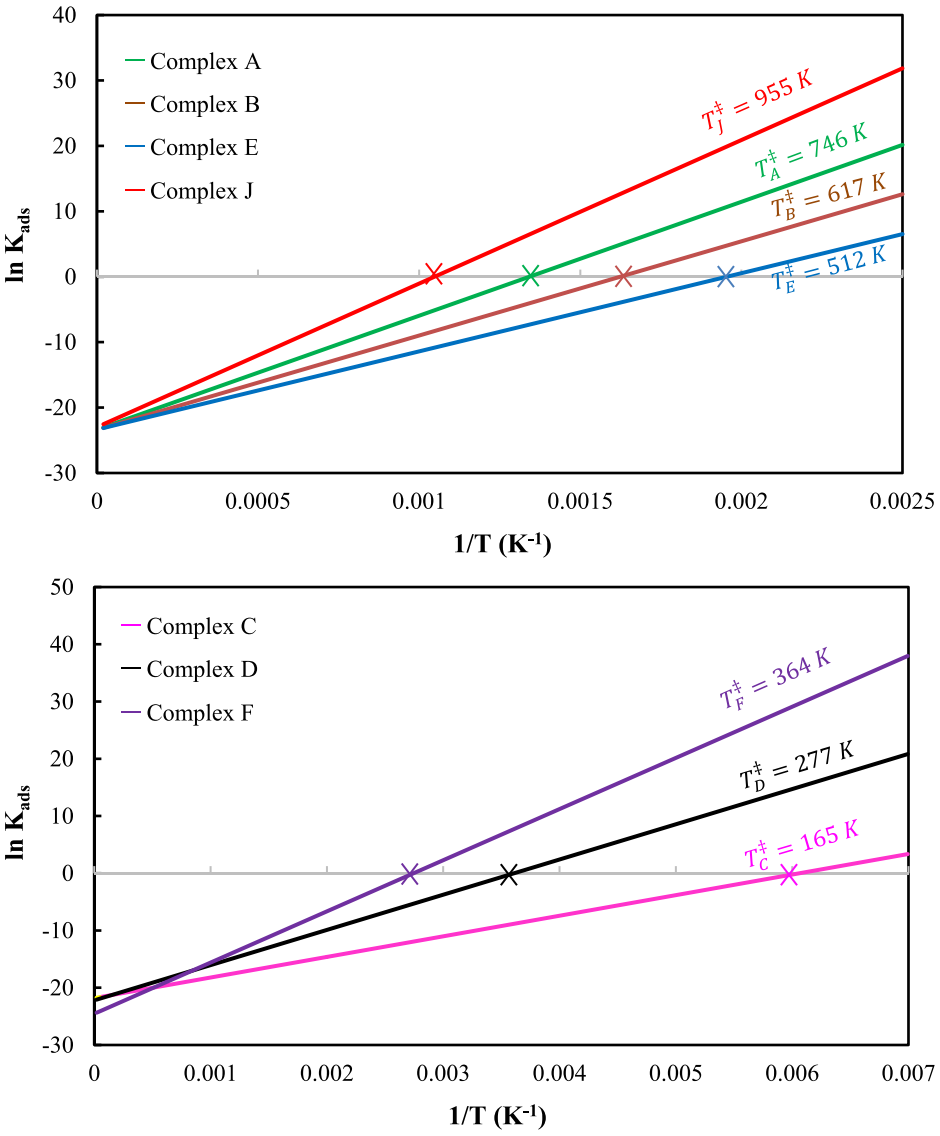

Fig. 4 Van 't Hoff plots for PCA/$B_{12}N_{12}$ and PCA/$B_{12}CaN_{12}$ systems at different adsorption configurations.

cally favored ($lnK_{ads} > 0$) except for Complex C and D which are entropically favored ($lnK_{ads} < 0$). The values of T_i^{+} show that only Complex A (746 K), B (617 K), E (512 K), F (364 K) and J (955 K) are able to remain thermodynamically favored above 298 K. At temperature beyond T_i^{+}, the adsorption becomes unfavorable, thus reducing the formation and stability of the adsorption of complexes. The van't Hoff plots also show the most stable adsorption complex across the largest temperature range in ~~is~~ Complex J which is PCA/ $B_{12}CaN_{12}$ with amine as the adsorption head. Even though the adsorptions of PCA on both $B_{12}N_{12}$ and $B_{12}CaN_{12}$ are thermodynamically feasible ($\Delta_{ads}G < 0$) but PCA has a higher adsorption preference on $B_{12}CaN_{12}$ ($\Delta_{ads}G = -1.30eV$) than $B_{12}N_{12}$ ($\Delta_{ads}G = -0.90eV$). This finding supports the previous discussion on the ability of intercalated calcium ion in stabilizing adsorption complex by attracting PCA to nanocage surface via its positive charge.

3.3. Electronic properties

Electronic properties of PCA and adsorption complexes were examined via frontier molecular orbital plots. In Fig. 1, the frontier molecular orbital (FMO) plot of neutral PCA molecule shows that the highest occupied molecular orbital (HOMO) and lowest unoccupied molecular orbital (LUMO) are mainly distributed for amine and thiol groups; carbonyl and hydroxyl groups respectively which are the main sites involved in the charge transfer for zwitterionic form. In the absence of PCA interaction, the intercalation of calcium ion in $B_{12}N_{12}$ nanocage has significantly altered its electronic features as evidenced by the change in HOMO distribution from an equal distribution across nanocage to a localized distribution at the displaced B-N bond (Fig. 2). Similar observation was also reported in other work where the displacement of HOMO and LUMO of $B_{12}N_{12}$ fullerene was generated by chemical disorder, thus forming potential reactive sites for

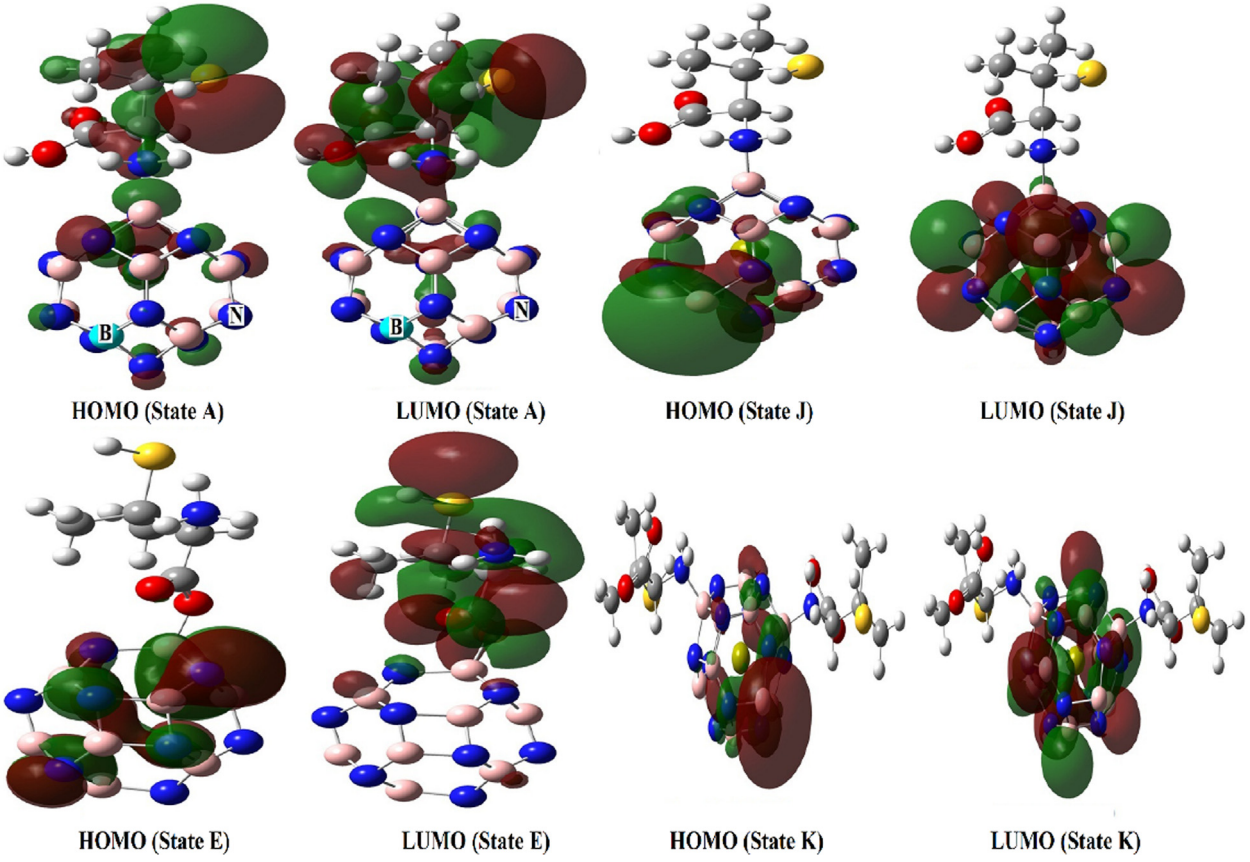

Fig. 5 FMO plots of PCA/$B_{12}N_{12}$ (A and E) and PCA/ $B_{12}CaN_{12}$ (J and K) complexes.

external molecules. Likewise, the HOMO-LUMO energy gap was also significantly reduced by more than half of its initial value: 9.51 eV to 3.46 eV and 9.48 eV to 3.22 eV for aqueous and chloroform environments, respectively. This indicates an increase in the chemical reactivity and the electrical conductivity via calcium functionalization.

FMO plots in Fig. 5 indicate the hybridization of HOMO and LUMO of PCA and $B_{12}N_{12}$ nanocage during interaction. The HOMO and LUMO are now mainly distributed over $B_{12}N_{12}$ nanocage and PCA molecule respectively which is due to electron transfer from PCA molecule to $B_{12}N_{12}$ nanocage during interaction. The hybridization was also in tandem with the increase in HOMO energies from −9.44 eV to the range of −8.71 eV – −7.63 eV which subsequently reduces the energy gap of the adsorption complexes. Similar hybridization trend was also reported in other works using adsorbents such as C_{20} (Alireza Soltani et al., 2020) and $B_{12}N_{12}$ (Hoseininezhad-Namin et al., 2020). Several LUMOs were observed to have positive energies which indicate their antibonding nature (Soltani et al., 2018). For PCA/ $B_{12}CaN_{12}$ systems, the electron transfers were more significant to the extent of the hybridized LUMO being localized at the nanocage. The close proximity of HOMO and LUMO in this system also accounts for the significant reduction in energy gap that improves its electronic interaction with PCA.

Tables 1 and 2 show the quantum molecular descriptors of PCA, nanocage and adsorption complexes. By functionalizing $B_{12}N_{12}$ nanocage with calcium ion, a significant reduction (range of 60%) in HOMO-LUMO energy gap has enabled a more facile electron transition thus increasing its reactivity for PCA interaction. This effect is reflected in the increase of global softness (0.105 eV^{-1} to 0.316 eV^{-1} or 0.311 eV^{-1}) and the decrease in global hardness (4.76 eV to 1.58 eV and 4.74 eV to 1.61 eV) and electronic chemical potential (−4.69 eV to −2.89 eV and −4.70 eV to −2.94 eV) of $B_{12}CaN_{12}$ nanocage in the respective aqueous and chloroform environments. Upon interaction, HOMO-LUMO energy gap of adsorption complexes were also notably reduced within the approximate range of 1% to 18%. This change would also predict the increase in chemical reactivity of adsorption complexes as reflected in the increase of global softness and the decrease in global hardness and electronic chemical potential values.

Some slight variations of quantum molecular descriptors were also noted when adsorption configurations were altered. During interaction, the hybridization of HOMO and LUMO is very much dependent on the spatial arrangement of the existing HOMO and LUMO. Therefore, a change in adsorption configuration would have spatial effect on the energy gap (E_g) which then results in variation of chemical properties of the system. This spatial effect is only obvious when the adsorption configuration change involves a sideways position swapping between thiol-amine pair (HOMO region) and carbonyl-hydroxyl pair (LUMO region) relative to the position of $B_{12}N_{12}$ nanocage. Thus, a change in adsorption configuration from amine (A) to thiol (D) group or vice versa has negligible change on the energy gap and their quantum molecular descriptors as the HOMO-LUMO positions of PCA relative to

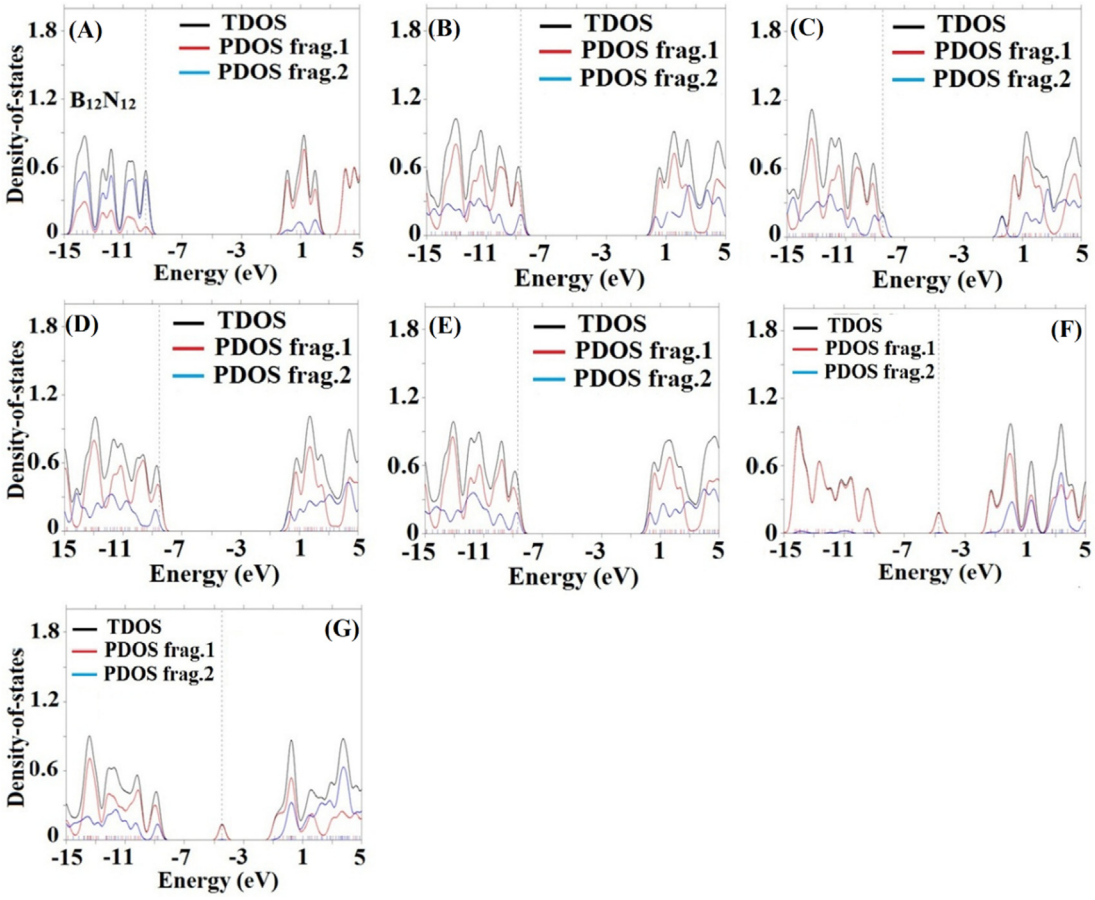

Fig. 6 PDOS and TDOS plots for bare $B_{12}N_{12}$ (A), States A, B, E and F (B-E), $B_{12}CaN_{12}$ (F) and State J (G).

the HOMO-LUMO positions of $B_{12}N_{12}$ nanocage remain unaltered. Similar observation was also noted if one were to change the adsorption configuration between carbonyl (B) and hydroxyl (C) groups. It is only when the change occurs across these two pair groups then the HOMO-LUMO hybridization is spatially affected and hence altering the chemical properties of the adsorption complexes.

The total density of states (TDOS) and projected density of state (PDOS, Fragments) for the selected adsorption configurations (A, B, E and F) were performed and analyzed to further realize the nature of the binding between the PCA and the $B_{12}N_{12}$ and $B_{12}CaN_{12}$ nanocages are depicted in Fig. 6. Projected density of state plots of first (nanocage) and second (drug) fragments were represented with the respective red and blue colors of determined systems. The vertical line shows the position of the Fermi level (E_F) and the edge of the valance band. Different states of the PDOS precisely represent the dependency of the electronic property of interaction systems to the spectral adsorption position and orientation of PCA interaction with the pristine and $B_{12}CaN_{12}$ nanocages. In Tables 1 and 2, significant changes have been happened in the energy of the donor and acceptor states in complexes B and G.

The electron localization function (ELF) topology of the most stable interaction configurations was computationally modeled. The ELF space contour maps for the PCA molecule interacted with the $B_{12}N_{12}$ and $B_{12}CaN_{12}$ nanocages are presented in Fig. 7. The ELF provides a good picture of the electron space delocalization between the adsorbate and adsorbent (Hoseininezhad-Namin et al., 2020; Soltani et al., 2018). It shows the jellium–like homogeneous electron gas and renormalizes the value between 0.00 and 1.00 herein the value 1.0 represents a strong localization (red areas) while 0.50 and 0.00 values attribute to free electron gas behavior (green areas) and zero localization, respectively (Xu et al., 2018; Guo et al., 2015). It is clear that a significant localization (red areas) of electron happened between different functionalities (through O or N atoms) of the PCA molecule and the B atom of the $B_{12}N_{12}$ nanocage upon adsorption which agrees on the formation of a covalent band between the two species (States A-D). However, after Ca entrapment, the ELF topology of the $B_{12}N_{12}$ nanocage changes and creates a more localization around the Ca atom which already shown formation of the chemical bonds with $B_{12}N_{12}$ nanocage (state X and Y). Herein, interaction of the PCA molecule through its amine group to the $B_{12}CaN_{12}$ nanocage even create a more reddish area

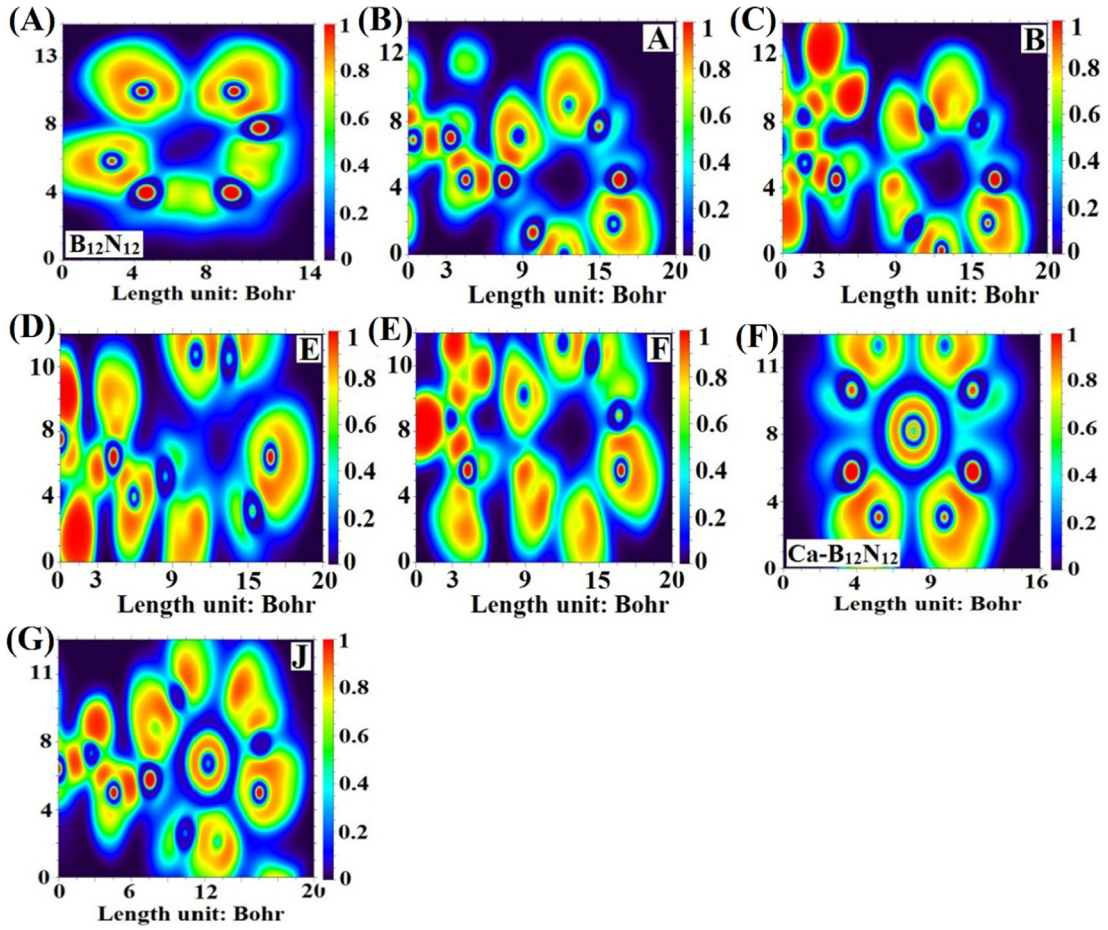

Fig. 7 Electron Localization Function plots for bare $B_{12}N_{12}$ (A), States A, B, E and F (B-E) $B_{12}CaN_{12}$ (F) and the State J (G).

(strong localization) at the area where the adsorption happens (State J). This signifies Ca entrapment can enhance the binding energy of the covalent bond formed between two species as evidenced earlier by the larger binding energy values.

3.4. Molecular docking

Molecular docking analysis was carried out to study the binding affinity of the PCA/$B_{12}N_{12}$ and PCA/$B_{12}CaN_{12}$ bio-nanostructures against the tumour necrosis factor alpha and interleukin-1 receptor targets via the AutoDock (4.2) software (Mohan and Yu, 2011; Shaki et al., 2020). To investigate the inhibition mechanism of tumour necrosis factor alpha (TNF-α) receptor, the optimized configurations (state E, J, A, and PCA) were undertaken molecular docking in the binding pocket of TNF-α receptor protein. The PCA (NH_2)/$B_{12}N_{12}$ (State J) is found as the most potent inhibitor of the TNF-α compared to other studied bio-nanostructures. The binding energies of −10.3, −9.8, −10.7 and −7.5 kcal/mol were calculated for the state E, J, A, and PCA, −10.3, −9.8, −10.7 and −7.5 kcal/mol, in the binding pocket of the docked protein (Table 4). State J is stabilized in the binding pocket of tumor necrosis factor alpha receptor by hydrophobic interactions with different amino acid residues like Tyr119, Leu120, Tyr59, Tyr15 and Gly121 in chain A and also Tyr151, Leu120, Tyr59, Tyr119 and Gly121 in chain B. Moreover, the complex was bond with Ser60, Gln61 in chain A and Ser60 in chain B via polar interactions. Furthermore, the complex is stabilized in the binding pocket of receptor (PDB ID: 2AZ5) by five hydrogen bonds with the residues of protein such as Tyr151, Ser60, Leu120 where the hydrogen bond lengths were 1.43 Å, 1.63 Å, 3.01 Å, 3.29 Å and 3.88 Å respectively. Previous study has proven that, amino acid residues Tyr59, Tyr151, Leu120, Ser60 and Gln61 were the key amino acids in the active site of target (Aghaei et al., 2021) and the obtained results demonstrated that the State J was bond with analogous amino acid residues in the active site resulting in the inhibition of the TNF-α receptor (Fig. 8A and B).

The computed binding energies of the States E, J, A, and PCA in the binding pocket of the IL-1beta receptor protein were −8.8, −8.1, −9.3 and −6.3 kcal/mol respectively (Table 4). Furthermore, State J was stabilized in the binding pocket of the target via hydrophobic interactions with different amino acid residues like Ala51, Val52, Ile74 and Leu79 (Fig. 8C and D). Moreover, amino acid residues such as Asp49, Glu50, Arg34, Lys53, Glu94 and Lys76 interacted with the target via electrostatic interactions. The obtained results show that State J interacted with the key amino acid residues such as Arg34, Asp49 and Glu50 in the active site and result in the inhibition of the IL-1 receptor. The complex was also stabilized in the binding pocket of receptor (PDB ID: 2L5X) by four hydrogen bonds with the residues of protein such as

Table 4 Molecular docking simulations results

Compound	TNF-α receptor (PDB ID: 2AZ5)		IL-1 receptor (PDB ID:2L5X)	
	Binding energy(kcal/mol)	K_i (μM)	Binding energy(kcal/mol)	K_i (μM)
State E	−10.3	3.3	−8.8	7.8
State J	−9.8	7.3	−8.1	8.4
State A	−10.7	5.1	−9.3	6.3
PCA	−7.5	10.7	−6.3	14.2

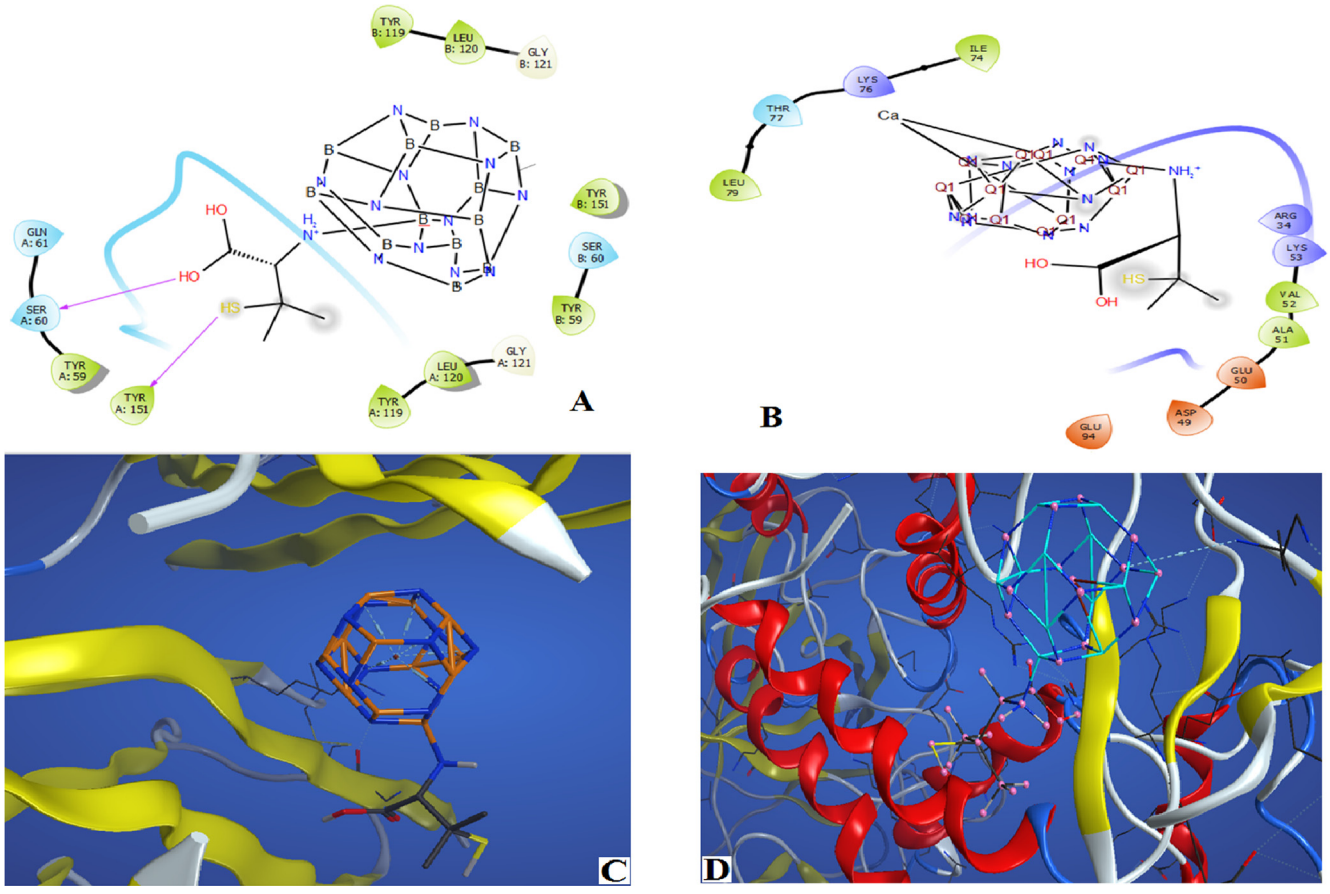

Fig. 8 Presentation of 2D (A, C) and 3D (B, D) models of interactions between PCA from its NH_2 group with $B_{12}N_{12}$ and $B_{12}CaN_{12}$ surfaces on TNF receptor (PDB ID: 2AZ5) and IL-1 receptor (PDB ID: 2L5X), respectively.

Arg34, Thr77 and Lys76 where hydrogen bond lengths were 3.06 Å, 3.14 Å, 1.94 Å and 2.87 Å respectively. The 3D model for the binding mode indicated that the complex is buried in the pockets of the IL-1 receptor (Fig. 8C and D). A comparison of molecular docking calculations demonstrated that the State A had high binding energy to the target molecule while suggesting a strong binding with other potential targets and inhibits more efficiently the active site of the protein than the other states (Gong et al., 2018; Srivastava et al., 2020). Molecular docking analysis shows that the State A could be a potential inhibitor of the TNF-α and IL-1 receptor at the binding site. The inhibition constant Ki(μM) were also calculated and represented in Table 4. It illustrates how potent the Sates A and E are as an inhibitor where the lower the value of Ki the higher the inhibiting character of the compound [80]. Therefore, our studies reveal the inhibiting characteristic of the calculated states as Sate A > Sate E > Sate J towards the TNF receptor (PDB ID: 2E7A) and IL-1 receptor (PDB ID: 2L5X).

3.5. Drug likeness and ADMET prediction

We selected ligand molecules, and then analyzed them for accepting to understand their compliance with *Lipinski's Rule of Five*. States A and J complied the standardized rule thus were chosen to consider additionally (Table 5). As indicated in Table 5, the majority of structures obey Lipinski's "Rule of Five". The log P values for the states A and J were calculated to be −2.31 and −2.32 (unit), (Table 5) whereas the log

Table 5 Drug-likeness properties of compounds.

Property	MW	log S	log P	HBA	HBD	Number of rotatable bonds	Molecular refractivity	TPSA	Drug likeness
ref	–	less than140	40–130	< = 10	< = 12	< = 12	< = 5	> -4	
PCA	151	0.87	63	38.7	2	3	3	0.11	0.49
State A	449	0.54	128	176.1	4	2	14	−2.31	−3.11
State E	447	0.61	63.3	176	4	1	14	−2.31	−4.06
State J	487	0.68	129	176.4	4	2	14	−2.32	−3.12

Abbreviations: MW as molecular weight; log S as logarithm of water solubility; log P as logarithm of compound partition coefficient between n-octanol and water; HBA as number of hydrogen bonds acceptors; HBD as number of hydrogen bond donors; TPSA as topological polar surface area.

Table 6 ADMET profile of compounds.

Compound	BBB	HIA	Caco2	P-glycoprotein inhibitor	CYP450-2C9	CYP450-2D6	CYP450-3A4	AMES	Carcinogens	Hepatotoxicity	Acute oral Toxicity (kg/mol)
ref	–	Non toxic	Non carcinogen	Non Ames toxic	Non-inhibitor	Non-inhibitor	Non-inhibitor	Non inhibitor	–	–	–
PCA	0.69	Non toxic	Non carcinogen	Non Ames toxic	Non inhibitor	Non inhibitor	Non inhibitor	Non inhibitor	No	Yes	No
State A	0.51	Non toxic	Non carcinogen	Non Ames toxic	Non inhibitor	Non inhibitor	Non inhibitor	Non inhibitor	No	Yes	No
State E	0.53	Non toxic	Non carcinogen	Non Ames toxic	Non inhibitor	Non inhibitor	Non inhibitor	Non inhibitor	No	Yes	No
State J	0.55	Non toxic	Non carcinogen	Non Ames toxic	Non inhibitor	Non inhibitor	Non inhibitor	Non inhibitor	No	Yes	No

Abbreviations: BBB: Blood Brain Barrier; HIA: Human Intestinal Absorption.

S values of −3.11 and −3.12 (unit) were determined for these states, respectively. Furthermore, the log P and log S values for the PCA were obtained to be 0.11 and 0.49 (unit), respectively. The Topological polar surface area (TPSA) values for the PCA increases from 63 to 128 (state A) and 129 (state J) upon interaction of the PCA on the $B_{12}N_{12}$ and $B_{12}CaN_{12}$ nanocages. Herein, larger TPSA value is related with the least permeability of the membrane and a compound is considered a better sorbate for *p*-glycoprotein if its TPSA values get bigger upon adsorption or any chemical process which is liable for efflux of drug from the cell and conversely the reduced TPSA value is beneficial for drug-like property (Srivastava et al., 2020).

The oral bioavailability measures are implemented to the whole tested systems, possessing lower than 10 rotating bonds, thus they are less flexible in terms of configuration. The molar refractivity of compound PCA is less than 130 and the others have higher values. Topological polar surface area (TPSA), i.e., the surface that belongs to polar atoms, is a describer having a good correlation with passive molecular transfer via membranes, such as BBB. All compounds possess TPSA values lower than 140 Å, and the water solubility of all compounds were taken as moderately soluble (see Table 5). Additionally, selected molecules underwent the evaluation of their potentiality for ADMET profiles (Table 6). High intestinal absorption and low oral bioavailability were obtained in the whole structures. All compounds had no Caco-2 penetrability, while most of them are non-inhibitors of membrane *p*-glycoproteins and all compounds cannot penetrate BBB. Furthermore, most compounds were reported to be non-inhibitor of CYP (CYP3A4, CYP2D6, and CYP2C9) as well as non-AMES toxicity, hepatotoxicity and non-carcinogenic.

4. Conclusions

DFT calculations of penicillamine on pure and calcium entrapped $B_{12}N_{12}$ nanocages were carried out in aqueous and chloroform solvents. It was found that the adsorption of PCA on $B_{12}N_{12}$ nanocages are in the chemisorption regime and occurs via its four nucleophilic sites: amine, carbonyl, hydroxyl, and thiol. The most stable adsorption configuration was achieved when zwitterionic PCA adsorbs via its amine group. Our results also reveal that PCA adsorption in a solvent environment could be further stabilized by solvent of higher hydrogen bond strength and polarity. These solvent–solute bonds aided in reducing the partial charges of PCA and their availabilities for electron acceptance. The functionalization of $B_{12}N_{12}$ nanocage with calcium ion shows an enhanced stability and adsorption capacity of the PCA/Ca-$B_{12}N_{12}$ complex. The intercalated calcium ion was shown to attract PCA molecules to nanocage surface via its positive charge. Our study demonstrates that the adsorption energy of PCA is negative in the exothermic process (State J), with values of −2.162 eV in aqueous solvent and −2.230 eV in chloroform solvent. The results exhibit that the PCA drug via their amine and carbonyl groups were covalently bonded to the nanocage surface, whereas the hydroxyl and thiol groups represent weak interactions due to noncovalent bonds between the two species. Molecular docking study indicates that the state A has a good binding affinity with TNF-α and IL-1 receptor protein recep-

tors in comparison with the other compounds. The possible survival of a compound in the later phases of developing drugs was determined through *in silico* assay of absorption, distribution, metabolism, excretion, and toxicity (ADMET) as well as drug-likeness. The obtained results of drug-likeness and ADMET properties revealed that state A had good ADMET properties relative to the others and had potential inhibition of inflammation, which has the potential of extra optimization as a key compound.

Declaration of Competing Interest

The authors declare that they have no known competing financial interests or personal relationships that could have appeared to influence the work reported in this paper.

Acknowledgements

We gratefully acknowledge financial support from Golestan University of Medical Science (Research Project Grant No. 980308035).

References

Abdolahi, N., Aghaei, M., Soltani, A., Azmoodeh, Z., Balakheyli, H., Heidari, F., 2018. Adsorption of celecoxib on B12N12 fullerene: spectroscopic and DFT/TD-DFT study. Spectrochim. Acta A Mol. Biomol. Spectrosc. 204, 348–353.

Abdolahi, N., Aghaei, M., Soltani, A., Azmoodeh, Z., Balakheyli, H., Heidari, F., 2018. Adsorption of celecoxib on $B_{12}N_{12}$ fullerene: spectroscopic and DFT/TDDFT study. Spectrochim. Acta A 204, 348–353.

Abdolhi, N., Soltani, A., Khandan Fadafan, H., Erfani-Moghadam, V., Dehno Khalaji, A., Balakheyli, H., 2017. Preparation, characterization and toxicity evaluation of Co3O4 and NiO-filled multi-walled carbon nanotubes loaded to chitosan. Nano-Structures & Nano-Objects 12, 182–187.

Aghaei, M., Ramezanitaghartapeh, M., Javan, M., Hoseininezhad-Namin, M.S., Mirzaei, H., Shokuhi Rad, A., Soltani, A., Sedighi, S., A. Ng Kay Lup, V. Khori, P.J. Mahon, F. Heidari, 2021. Investigations of adsorption behavior and anti-inflammatory activity of glycine functionalized Al12N12 and Al12ON11 fullerene-like cages. Spectrochim. Acta, Part A 246, 119023.

Alireza Soltani, M., Ramezanitaghartapeh, M.B., Javan, M.T., Baei, A.N.K., Lup, P.J., Mahon, M. Aghaei, 2020. Influence of the adsorption of toxic agents on the optical and electronic properties of B12N12 fullerene in the presence and absence of an external electric field. New J. Chem. 44, 14513.

Ammar, H.Y., Badran, H.M., Umar, A., Fouad, H., Alothman, O.Y., 2019. ZnO nanocrystal-based chloroform detection: density functional theory (DFT) study. Coatings 9, 769.

Baei, M.T., Ramezani Taghartapeh, M., Tazikeh Lemeski, E., Soltani, A., 2014. A computational study of adenine, uracil, and cytosine adsorption upon AlN and BN nanocages. Phys. B 444, 6–13.

Bezi Javan, M., Soltani, A., Azmoodeh, Z., Abdolahi, N., Gholami, N., 2016. A DFT study on the interaction between 5-fluorouracil and B12N12 nanocluster. RSC Adv. 6, 104513–104521.

Bezi Javan, M., Soltani, A., Tazikeh Lemeski, E., Ahmadi, A., Moazen Rad, S., 2016. Interaction of $B_{12}N_{12}$ nano-cage with cysteine through various functionalities: a DFT study. Superlattice Microstruct. 100, 24–37.

Bieri, M., Thomas Bürgi, 2006. D-Penicillamine Adsorption on Gold: An in Situ ATR-IR Spectroscopic and QCM Study. Langmuir 22, 8379–8386.

Blaudeau, J.P., McGrath, M.P., Curtiss, L.A., Radom, L., 1997. J. Chem. Phys. 107, 5016–5021.

Buzatu, D.A. et al, 2009. Nanotubes for cancer therapy and diagnostics. US patent 7608240.

Carreto Escobar, J., Salazar Villanueva, M., Bautista Hernández, A., Cortés-Arriagada, D., Chigo Anota, E., 2019. Interactions of $B_{12}N_{12}$ fullerenes on graphene and boron nitride nanosheets: A DFT study. J. Mol. Graph. Model. 86, 27–34.

Cazorla, C., Rojas-Cervellera, V., Rovira, C., 2012. Calcium-based functionalization of carbon nanostructures for peptide immobilization in aqueous media. J. Mater. Chem. 22, 19684–19693.

Chen, Y., Zou, J., Campbell, S.J., Le Caer, G., 2004. Boron nitride nanotubes: Pronounced resistance to oxidation. Appl. Phys. Lett. 84, 2430–2432.

Chigo Anota, E., Cocoletzi, G.H., 2014. GGA-based analysis of the metformin adsorption on BN nanotubes. Physica E 56, 134–140.

Chigo Anota, E., Bautista Hernández, A., Escobedo Morales, A., Castro, M., 2017. Design of the magnetic homonuclear bonds boron nitride nanosheets using DFT methods. J. Mol. Graph. Model. 74, 135–142.

Choy, E., Panayi, G., 1999. Mechanisms of action of second-line agents and choice of drugs in combination therapy. Clin. Exp. Rheumatol. 17, S20–S28.

Ciofani, G. et al, 2009. Boron nitride nanotubes: a novel vector for targeted magnetic drug delivery. Curr. Nanosci. 5, 33–38.

Ciofani, G., Danti, S., D'Alessandro, D., Moscatoc, A., Menciassi, S., 2010. Biochem. Biophys. Res. Commun. 394, 405.

Ciofani, G., Danti, S., Genchi, G.G., D'Alessandro, D., Pellequer, J.-L., Odorico, M., Mattoli, V., Giorgi, M., 2012. Pilot in vivo toxicological investigation of boron nitride nanotubes. Int. J. Nanomed. 7, 19–24.

Duverger, E., Balme, S., Bechelany, M., Miele, P., Picaud, F., 2019. Natural payload delivery of the doxorubicin anticancer drug from boron nitride oxide nanosheets. Appl. Surf. Sci. 475, 666–675.

Ebrahimi, J., Ghorbanzadeh Ahangari, M., Jahanshahi, M., 2018. Computational studies at the density functional theory (DFT) level about the surface functionalization of hexagonal monolayers by chitosan monomer. Appl. Surf. Sci. 440, 778–789.

Emanet, M., Çobandede, Z., Çulha, M., 2015. Interaction of carbohydrate modified boron nitride nanotubes with living cells. Colloids Surf B Biointerfaces. 134, 440–446.

Ferreira, T.H., Soares, D.C.F., Moreira, L.M.C., Silva, P.R.O., Santos, E.M.B., Sousa, R.G., Mater. Sci. Eng. C Mater. Biol. Appl. (33 2013) 4616.

Ferreira, T., Silva, P.R.O., Santos, E.M.B., Sousa, R.G., 2011. J. Biomater. Nanobiotechnol. 2, 426.

Ghasemi, A.S., Mashhadban, F., Ravari, F., 2018. A DFT study of penicillamine adsorption over pure and Al-doped C_{60} fullerene. Adsorption 24, 471–480.

Ghasemi, A.S., Ramezani Taghartapeh, M., Soltani, A., Mahon, P.J., 2019. Adsorption behavior of metformin drug on boron nitride fullerenes: thermodynamics and DFT studies. J. Mol. Liq. 275, 955–967.

Golberg, D., Bando, Y., Huang, Y., Terao, T., Mitome, M., Tang, C., Zhi, C., 2010. Boron nitride nanotubes and nanosheets. ACS Nano 4, 2979–2993.

Gong, E.C., Chea, S., Balupuri, A., Kang, N.S., Chin, Y.W., Choi, Y. H., 2018. Enzyme kinetics and molecular docking studies on cytochrome 2B6, 2C19, 2E1, and 3A4 activities by sauchinone. Molecules 23, 555–570.

Guo, Z., Li, B., Cheng, L.-T., Zhou, S., Andrew McCammon, J., Che, J., 2015. Identification of protein−ligand binding sites by the level-set variational implicit-solvent approach. J. Chem. Theory Comput. 11, 753–765.

He, M.M., Smith, A.S., Oslob, J.D., Flanagan, W.M., Braisted, A.C., Whitty, A., et al, 2005. Small-molecule inhibition of TNF-alpha. Sci. (New York, NY). 310 (5750), 1022–1025.

Horvath, L., Magrez, A., Golberg, D., Chunyi, Z., Bando, Y., Samajda, R., Horvath, E., Forro, L., Schwaller, B., 2011. ACS Nano 5, 3800.

Hoseininezhad-Namin, M.S., Pargolghasemi, P., Saadi, M., Ramezani Taghartapeh, M., Abdolahi, N., Soltani, A., Lup, A.N.K., 2020. Ab initio study of TEPA adsorption on pristine, Al and Si doped carbon and boron nitride nanotubes. J. Inorg. Organomet. Polym. 30, 4297–4310.

Jamroz, M.H., Vibrational Energy Distribution Analysis VEDA 4, Warsaw, 2004-2010

Joly, D., Rieu, P., Mejean, A., Gagnadoux, M.F., Daudon, M., Jungers, P., 1999. Pediatr. Nephrol. 13, 945.

Kim, H.A., Song, Y.W., 1997. Rheumatol. Int. 17, 5.

Kokalj, A., Behzadi, H., Farahati, R., 2020. DFT study of aqueous-phase adsorption of cysteine and penicillamine on Fe (110): Role of bond-breaking upon adsorption. Appl. Surf. Sci. 514, 145896.

Koopmans, T., 1933. Physica 1, 104.

Lahiri, D. et al, 2010. Boron nitride nanotube reinforced polylactide-polycaprolactone copolymer composite: mechanical properties and cytocompatibility with osteoblasts and macrophages in vitro. Acta Biomater. 6, 3524–3533.

Li, D., Hu, C., Luod, Y., Zhua, G., Li, Q., Luo, Z., Luo, K., 2019. One-pot synthesis of amphiphilic Janus gold nanoparticles with Dpenicillamine and benzyl mercaptan ligands by toluene/water emulsion reaction. Appl. Surf. Sci. 475, 615–620.

Mirmotahari, M., Sani, E., Rad, A.S., Khalilzadeh, M.A., 2019. Calcium-doped single-wall nanotubes (Ca/SWCNTs) as a superior carrier for atropine drug delivery: a quantum-chemical study in gas and solvent phases. J. Biomol. Struct. Dyn. 37 (16), 4267–4273.

Mirzaei, H., Keighobadi, M., Emami, S., 2017. An overview of anticancer chalcones with apoptosis inducing activity. J. Mazandaran Univ. Med. Sci. 26 (146), 254–268.

Mirzaei, H., Shokrzadeh, M., Emami, S., 2017. Synthesis, cytotoxic activity and docking study of two indole-chalcone derivatives. J. Mazandaran Univ. Med. Sci. 27 (154), 12–25.

Mohan, S.K., Yu, C., 2011. The IL1α-S100A13 heterotetrameric complex structure: a component in the non-classical pathway for interleukin 1α secretion. J. Biol. Chem. 286 (16), 14608–14617.

Morris, G.M., Huey, R., Lindstrom, W., Sanner, M.F., Belew, R.K., Goodsell, D.S., Olson, A.J., 2009. AutoDock4 and AutoDockTools4: Automated docking with selective receptor flexibility. J. Comput. Chem. 30 (16), 2785–2791.

Mortazavifar, A., Raissi, H., Akbari, A., 2019. DFT and MD investigations on the functionalized boron nitride nanotube as an effective drug delivery carrier for Carmustine anticancer drug. J. Mol. Liq. 276, 577–587.

Nagarajan, V., Chandiramouli, R., 2019. A study on quercetin and 5-fluorouracil drug interaction on graphyne nanosheets and solvent effects-A first-principles study. J. Mol. Liq. 275, 713–722.

Nejati, K., Hosseinian, A., Vessally, E., Bekhradnia, A., Edjlali, L., 2017. A comparative DFT study on the interaction of cathinone drug with BN nanotubes, nanocages, and nanosheets. Appl. Surf. Sci. 422, 763–768.

Padash, R., Sobhani-Nasab, A., Rahimi-Nasrabadi, M., Mirmotahari, M., Ehrlich, H., Rad, A.S., Peyravi, M., 2018. Is it possible to use X12Y12 (X = Al, B, and Y = N, P) nanocages for drug-delivery systems? A DFT study on the adsorption property of 4-aminopyridine drug. Appl. Phys. A 124, 582.

Padasha, R., Rabbani Esfahani, M., Shokuhi Rad, A., 2020. The computational quantum mechanical study of sulfamide drug adsorption onto X12Y12 fullerene-like nanocages: detailed DFT and QTAIM investigations, doi.org/10.1080/07391102.2020.1792991.

Parr, R.G., Donelly, R.A., Levy, M., Palke, W.E., 1978. J. Chem. Phys. 68, 3801.

Parr, R.G., Szentpaly, L., Liu, S., 1999. J. Am. Chem. Soc. 121, 1922.

Raggi, G., Stace, A.J., Bichoutskaia, E., 2014. Polarisation charge switching through the motion of metal atoms trapped in fullerene cages. PCCP 16, 23869–23873.

Rassolov, V.A., Pople, J.A., Ratner, M.A., Windus, T.L., 1998. J. Chem. Phys. 109, 1223–1229.

Roosta, S., Hashemianzadeh, S.M., Ketabi, S., 2016. Encapsulation of cisplatin as an anti-cancer drug into boron-nitride and carbon nanotubes: Molecular simulation and free energy calculation. Mater. Sci. Eng., C 67, 98–103.

Schmidt, M.W., Baldridge, K.K., Boatz, J.A., Elbert, S.T., Gordon, M.S., Jensen, J.H., Koseki, S., Matsunaga, N.J., 1993. Comput. Chem. (Oxford) 11, 1347.

Seifert, G., Fowler, W.P., Mitchell, D., Porezag, D., Frauenheim, Th., 1997. Boron-nitrogen analogues of the fullerenes: electronic and structural properties. Chem. Phys. Lett. 268, 352–358.

Shafiei, F., Hashemianzadeh, S.M., Bagheri, Y., 2019. Insight into the encapsulation of gemcitabine into boron- nitride nanotubes and gold cluster triggered release: A molecular dynamics simulation. J. Mol. Liq. 278, 201–212.

Shaki, H., Raissi, H., Mollania, F., Hashemzadeh, H., 2020. Modeling the interaction between anti-cancer drug penicillamine and pristine and functionalized carbon nanotubes for medical applications: density functional theory investigation and a molecular dynamics simulation. Journal of Biomolecular Structure and Dynamics, J Biomol Struct Dyn. 38 (5), 1322–1334.

Shokuhi Rad, A., Aghaei, S.M., 2018. Potential of metalefullerene hybrids as strong nanocarriers for cytosine and guanine nucleobases: A detailed DFT study. Curr. Appl. Phys. 18, 133–140.

Smolarek, C., Stremmel, W., 1999. Zeitchrift Fur Gastroenterologie 37 (4), 293.

Soltani, A., Baei, M.T., 2019. A DFT study on structure and electronic properties of BN nanostructures adsorbed with dopamine. Computation 7, 61.

Soltani, A., Baei, M.T., Tazikeh Lemeski, E., Kaveh, S., Balakheyli, H., 2015. A DFT study of 5-Fluorouracil adsorption on the pure and doped BN nanotubes. J. Phys. Chem. Solids 86, 57–64.

Soltani, A., Sousaraei, A., Bezi Javan, M., Eskandari, M., Balakheyli, H., 2016. Electronic and optical properties of 5-AVAfunctionalized BN nanoclusters: a DFT study. New J. Chem. 40, 7018–7026.

Soltani, A., Sousaraei, A., Bezi Javan, M., Eskandaric, M., Balakheyli, H., 2016. Electronic and optical properties of 5-AVA functionalized BN nanoclusters: a DFT study. New J. Chem. 40, 7018.

Soltani, A., Ramezanitaghartap, M., Javan, M.B., Mahon, P.J., Azmoodeh, Z., Tazikeh Lemeski, E., Kityk, I.V., 2018. Theoretical studies of hydrazine detection by pure and Al defected MgO nanotubes. Physica E 97, 239–249.

Soltani, A., Ramezani Taghartapeh, M., Erfani-Moghadam, V., Bezi Javane, M., Heidari, F., Aghaei, M., Mahon, P.J., 2018. Serine adsorption through different functionalities on the $B_{12}N_{12}$ and Pt-$B_{12}N_{12}$ nanocages. Mater. Sci. Eng., C 92, 216–227.

Srimathi, U., Nagarajan, V., Chandiramouli, R., 2018. Interaction of Imuran, Pentasa and Hyoscyamine drugs and solvent effects on graphdiyne nanotube as a drug delivery system-A DFT study. J. Mol. Liq. 265, 199–207.

Srivastava, V., Yadav, A., Sarkar, P., 2020. Molecular docking and ADMET study of bioactive compounds of glycyrrhiza glabra against main protease of SARS-CoV2. Mater. Today:. Proc. https://doi.org/10.1016/j.matpr.2020.10.055.

Sui, B., Liu, X., Sun, J., 2018. Dual-functional dendritic mesoporous bioactive glass nanospheres for calcium-influx mediated specific tumor-suppression and controlled drug delivery in vivo. ACS Appl. Mater. Interfaces 10 (28), 23548–23559.

Vatanparast, M., Shariatinia, Z., 2019. Hexagonal boron nitride nanosheet as novel drug delivery system for anticancer drugs: Insights from DFT calculations and molecular dynamics simulations. J. Mol. Graph. Model. 89, 50–59.

Vessally, E., Esrafili, M.D., Nurazar, R., Nematollahi, P., Bekhradnia, A., 2017. A DFT study on electronic and optical properties of aspirin-functionalized $B_{12}N_{12}$ fullerene-like nanocluster. Struct. Chem. 28, 735–748.

Xu, Z., Meher, B.R., Eustache, D., Wang, Y., 2014. Insight into the interaction between DNA bases and defective graphenes: covalent or non-covalent. J. Mol. Graph. Model. 47, 8–17.

Xu, S., Peng, H., Wang, N., Zhao, M., 2018. Inhibition of TNF-α and IL-1 by compounds from selected plants for rheumatoid arthritis therapy: In vivo and in silico studies. Trop. J. Pharm. Res. 17 (2), 277–285.

Yamanaka, H., Hakoda, M., Kamatani, N., Kashiwazaki, S., Carson, D.A., 1993. Formation of DNA strand breaks by D-penicillamine and bucillamine in human lymphocytes. Immunopharmacology 26, 113–118.

Yongnian, Z., Bing, Z., Zhi, H., Yanchun, T., Guangtian, Z., 1998. Infrared spectroscopy investigation of cubic boron nitride films. Spectrosc. Lett. 31 (5), 945–954.

Zhao, Y., Schultz, N.E., Truhlar, G.D., 2006. Design of density functionals by combining the method of constraint satisfaction with parametrization for thermochemistry thermochemical kinetics, and noncovalent interactions. J. Chem. Theory Comput. 2, 364–382.

Zhu, H., Zhao, C., Cai, Q., Fu, X., Sheykhahmad, F.R., 2020. Adsorption behavior of 5-aminosalicylic acid drug on the B12N12, AlB11N12 and GaB11N12 nanoclusters: A comparative DFT study. Inorg. Chem. Commun. 114, 107808.